92 Mb/s Fat-Intrabody Communication (Fat-IBC) With Low-Cost WLAN Hardware

Pramod K. B. Rangaiah, *Member, IEEE*, Johan Engstrand, Ted Johansson, *Senior member, IEEE*, Mauricio D. Perez, *Member, IEEE* and Robin Augustine, *Member, IEEE*

***Abstract*— The human subcutaneous fat layer, skin and muscle together act as a waveguide for microwave transmissions and provide a low-loss communication medium for implantable and wearable body area networks (BAN).**

In this work, fat-intrabody communication (Fat-IBC) as a human body-centric wireless communication link is explored. To reach a target 64 Mb/s inbody communication, wireless LAN in the 2.4 GHz band was tested using low-cost Raspberry Pi single-board computers. The link was characterized using scattering parameters, bit error rate (BER) for different modulation schemes, and IEEE 802.11n wireless communication using inbody (implanted) and on-body (on the skin) antenna combinations. The human body was emulated by phantoms of different lengths. All measurements were done in a shielded chamber to isolate the phantoms from external interference and to suppress unwanted transmission paths.

The BER measurements show that, except when using dual on-body antennas with longer phantoms, the Fat-IBC link is very linear and can handle modulations as complex as 512-QAM without any significant degradation of the BER.

For all antenna combinations and phantoms lengths, link speeds of 92 Mb/s were achieved using 40 MHz bandwidth provided by the IEEE 802.11n standard in the 2.4 GHz band. This speed is most likely limited by the used radio circuits, not the Fat-IBC link.

The results show that Fat-IBC, using low-cost off-the-shelf hardware and established IEEE 802.11 wireless communication, can achieve high-speed data communication within the body. The obtained data rate is among the fastest measured with intrabody communication.

***Index Terms*— Body area networks (BAN), Body sensor networks (BSN), Intrabody communication (IBC), Bit Error Rate (BER), Signal-to-noise ratio (SNR), WLAN.**

I. Introduction

In recent years, body area networks (BAN) and body sensor networks (BSN) have due to their potential in health care, sports, and entertainment gained attention [1], [2]. BAN allows data to be shared between personal portable devices and sensors on the body and plays an important role in a number of biomedical applications that continuously measure human physiological data such as electrocardiogram (ECG), heart rate, blood pressure, and body temperature [3]. A health tracker can measure important parameters continuously, which is essential for patients with chronic diseases who are at risk and who need early warning and long-term treatment [4]. For wireless BAN (WBAN) [5], the IEEE 802.15 standards [6] for Internet of Things (IoT) protocols, which include low data rate wireless personal area networks (WPAN) such as Bluetooth, ZigBee, and Wireless HART, can be used with communication speeds in the order of a few Mb/s.

Intrabody communication (IBC) is short-range communication inside the human body, and allows wireless connection of sensors on/off the human body [7]. IBC can be deployed using a number of different techniques, such as galvanic coupling, capacitive coupling, ultrasound, and resonant coupling [8]. Most of these IBC techniques suffer from low bandwidth and short transmission distances although ultrasound can reach tens of Mb/s over very short distances [9], and capacitive coupling up to 150 Mb/s [10] using custom CMOS transceiver circuit designs. However, for capacitive coupling, a path through external ground is needed, thus the modification of the surroundings becomes essential.

Brain-computer interfaces (BCI) provide a direct communication link between the brain and an external device. BCI can be used to record, decode and stimulate neural activity, treat neurological disorders and restore lost functions in patients, such as allowing a person to control robotic arms or to generate synthetic speech with just their thoughts [11]. B-CRATOS — "Wireless Brain-Connect inteRfAce TO machineS" [12] — is an EU H2020 FET Open project that defines a new paradigm for future Brain-Machine interfaces by supporting wireless high data rate, low-latency two-way communication to establish real-time communication for streaming motor cortex data (read data rate $>$32 Mb/s) between brain and a peripheral prosthetic and from prosthetic proprioceptive sensors (write data rate $>$2 Mb/s) to somatosensory cortex using the Utah array from Blackrock Neurotech.

Fat-IBC [13] is a novel technique that can be used to connect devices wirelessly using microwave transmission through the human body fat layer, sandwiched between skin and muscle. Due to the lower relative permittivity and losses of fat with respect to skin and muscle [14], the fat layer can act as a waveguide for microwave transmissions and support low-loss communication for implantable and wearable body networks. The RF small-signal characteristics show that the

Manuscript received 18 March 2023; revised 1 June 2023; accepted 27 June 2023. Date of publication XX July 2023; date of current version 30 June 2023. This work was supported by the B-CRATOS European Union's Horizon 2020 research and innovation program under Grant Agreement No. 965044. *(Pramod K. B. Rangaiah and Johan Engstrand and Ted Johansson are co-first authors.) (Corresponding author: Robin Augustine.)*

The authors are with Division of Solid-State Electronics, Department of Electrical Engineering, Uppsala University, Box 65, SE-751 03 UPPSALA, Sweden (e-mail: robin.augustine@angstrom.uu.se).

Digital Object Identifier 00.0000/TBME.2023.0000000

fat channel can be used at least up to 8 GHz without any significant increase in insertion loss [15], [16].

To reach a data speed >32 Mb/s with Fat-IBC, wireless LAN (WLAN, i.e. the IEEE 802.11 group of standards [17]) together with 4G and low/midband 5G are viable alternatives among the established communication standards. To reach 64 Mb/s, we need to target IEEE 802.11n or higher [18].

The modulation coding scheme (MCS) systems in the IEEE 802.11 protocols define various combinations of parameters that together result in data rates of varying speed. The IEEE 802.11n standard defines eight MCS indices for the "high throughput" (HT) data rates with channel bandwidths of 20 MHz (HT20) and 40 MHz (HT40) in the 2.4 GHz band [19].

Table I lists the HT data rates (for the case of a single spatial stream with the default guard interval of 800 ns). For 64 Mb/s with HT20, we need to reach the highest modulation rate (64-QAM) and coding to achieve speeds faster than 64 Mb/s. If a 40 MHz bandwidth (HT40) can be used, such speeds can be reached already with 16-QAM.

TABLE I
HT MCS DATA RATES IN IEEE 802.11N FOR A SINGLE SPATIAL STREAM WITH A GUARD INTERVAL OF 800 NS

			Data rate (Mb/s)	
MCS index	Modulation	Coding	HT20	HT40
0	BPSK	1/2	6.5	13.5
1	QPSK	1/2	13.0	27.0
2	QPSK	3/4	19.5	40.5
3	16-QAM	1/2	26.0	54.0
4	16-QAM	3/4	39.0	81.0
5	64-QAM	2/3	52.0	108.0
6	64-QAM	3/4	58.5	121.5
7	64-QAM	5/6	65.0	135.0

Although the potential of Fat-IBC for intrabody communication has been demonstrated using small-signal characterization and low-speed data packet transmission [20], high-speed digital data communication through this link has yet to be demonstrated. This paper aims to explore Fat-IBC as a communication link with both inbody (implanted) and onbody (on the skin) antennas in the 2.4 GHz band inside the body, with the goal to reach 64 Mb/s end-to-end data communication.

II. Materials and Methods

To evaluate the potential of using Fat-IBC for high-speed data transmission, we used two types of antennas, as described in Section II-A, and three-layer phantoms that model the skin/fat/muscle layers, as described in Section II-B. The design of a shielded chamber for the phantom measurements is discussed in Section II-C, and in Sections II-D and II-E, the tools and procedures for the RF characterization and WLAN measurements are described.

A. Antennas

Two types of antennas were used in this study. To emulate inbody (implanted) antennas, topology-optimized planar antennas (TOPA) similar to Asan, et al. [21] were used, with the impedance of the TOPA matched to that of the fat tissue for the R-band frequencies (1.7–2.6 GHz) [22]. For the onbody (on the skin) antennas, we used a ring-shaped antenna design based on the gap-coupled concentric annular ring microstrip antenna (ARMSA) concept, as described by Kanaujia et al. [23]. The FR4 material, with a dielectric constant of 4.4, a loss tangent of 0.02, and a height of 1.6 mm, was chosen for its cost-effectiveness and favorable electrical properties. The antenna was encapsulated within a layer of polydimethylsiloxane (PDMS) to ensure biocompatibility. Electromagnetic simulations were performed using a three-layered human tissue model to optimize the antenna's performance at the desired frequency of 2.45 GHz.

B. Fat-IBC phantoms

This study uses phantoms with three layers, emulating skin, fat, and muscle, respectively. The phantoms are designed for 500 MHz–20 GHz frequency range and manufactured from semi-solid, low water content structures designed to emulate the properties of real human tissues according to the recipes in [24], [25]. The muscle and skin layers of the phantoms were fabricated in a clean room environment. The materials used were DI-water, n-propanol, canola oil, kerosene, gelatin, TX-151, surfactant, glycerine, dextrin, corn starch, salt, and sodium benzoate. The material compositions of the layers were varied to obtain diverse dielectric properties, which were measured using a Keysight 85070E slim probe [26]. The measurements were in good agreement with the reference data from the Istituto di Fisica Applicata "Nello Carrara" (IFAC) database for the 2.45 GHz frequency, which provides a benchmark for dielectric properties of biological tissues [14].

The tissues have low water contents, therefore the phantoms can be stored for long periods of time without drying out. For the fat layer, we employed vulcanized rubber with similar dielectric properties to human fat tissue, i.e. relative permittivity of 5.28 and conductivity of 0.1 S/m. Three-layer phantoms of 10, 20, and 30 cm were fabricated. The widths of all phantoms were 58 mm, the fat and muscle layer heights were 30 mm each, and the skin layer was approximately 2 mm thick. The dimensions are similar to our previous work [15], except that we earlier only used phantoms up to a length of 10 cm.

To assess the data transmission within the fat, three cases with different antenna configurations, as shown in Fig. 1, were used.

1) Case 1, inbody-to-inbody antennas: The TOPA antennas were used to emulate inbody (implanted) antennas, placed on both sides of the phantom, providing a good coupling of the signal from the antennas to the fat layer. The experimental setup is shown in Fig. 1(a) with fat channel lengths of 10, 20, and 30 cm. The TOPAs have to be carefully aligned with the phantom to avoid signal loss.

2) Case 2, inbody-to-onbody antennas: For this case, a TOPA to an onbody antenna configuration was used. However, signal coupling to the Fat-IBC channel with the onbody antenna is less efficient than with an inbody antenna. The experimental setup is illustrated in Fig. 1(b), with phantom lengths of 10, 20, and 30 cm.

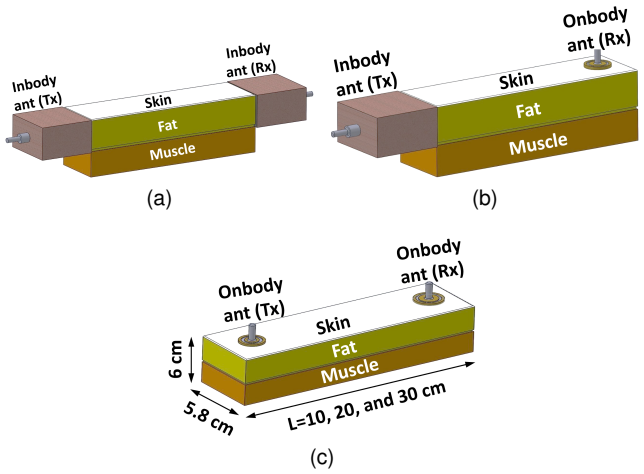

Fig. 1. Antenna connections to the phantoms: (a) Case 1: inbody-to-inbody antennas, (b) Case 2: inbody-to-onbody antennas, (c) Case 3: onbody-to-onbody antennas.

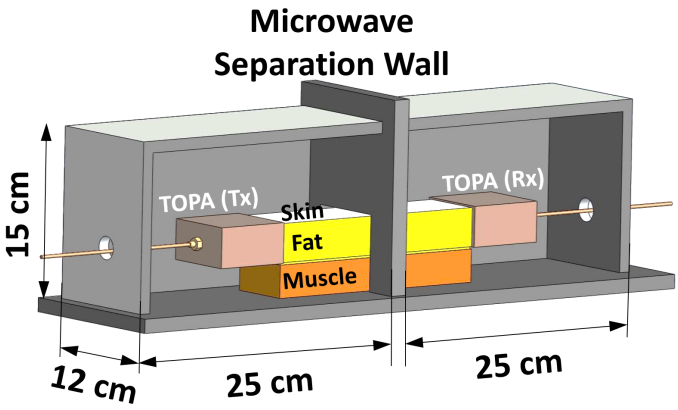

Fig. 2. A conceptual model of the shielded chamber, with two TOPAs and a phantom.

3) Case 3, onbody-to-onbody antennas: For the third case, both antennas were onbody antennas. The experimental setup is illustrated in Fig. 1(c), with phantom lengths of 10, 20, and 30 cm.

C. Design of a shielded chamber for phantom measurements

To reduce external interference, we used a shielded chamber, as sketched in Fig. 2. The chamber includes a wall to suppress surface waves, mainly at the air-skin interface. Interference from surface waves, as secondary (undesired) propagation paths, is expected to be more prominent for Case 2 and Case 3 due to the onbody antennas. With the separation wall, such surface waves are reduced for all cases equally [27].

The chamber consists of two rectangular cuboid-like 3D-printed plastic structures, parted by the removable separation wall. All internal faces of the cuboids and lateral faces of the separation wall are covered with high-loss 15-mm thick foam microwave absorbers (EA-LF500-24). The separation wall has overall dimensions of 18 × 15 × 2.5 cm, and protrudes slightly from the cuboids. A section at the bottom part of the separation wall is cut to fit the three-layer phantom. The external faces

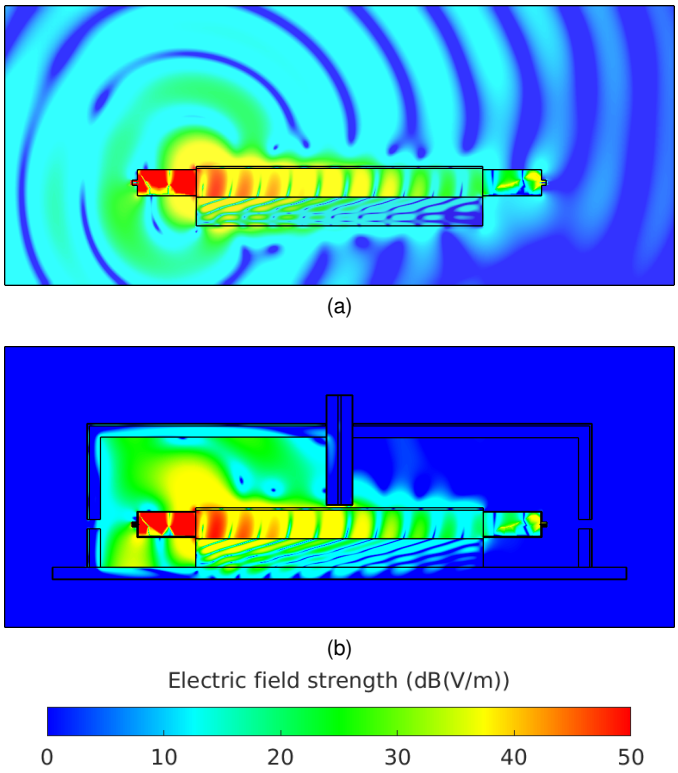

Fig. 3. Longitudinal-cutplane view of the simulated 3D electric field distribution at 2.45 GHz for Case 1 with a 30 cm phantom: (a) without the shielded chamber and wall and (b) with the shielded chamber and wall. The scale is clamped at 0 dB(V/m) and 50 dB(V/m).

of the chamber are clad with a 30-μm thick aluminium foil to enhance shielding efficiency.

To illustrate the shielding ability of the chamber, we used CST Microwave Studio 2021 to simulate the 3D electric field distribution for two instances of Case 1: one with the shielded chamber and wall and the other without them. The simulations included the TOPAs and a 30-cm phantom and were done with an "open" boundary. The phantoms were modelled based on dispersion data in the IFAC database [14].

To demonstrate the suppression ability of the wall, the suppression of a space wave and reduction of a surface wave when comparing the shielded and unshielded cases can clearly be seen in Fig. 3.

D. Radio equipment and parameter settings

Using the shielded chamber with the different phantoms and antenna combinations, the coupling of the signal from the antennas to the fat channel and the losses through the channel were evaluated by small-signal scattering parameters (s-parameters) between 2 and 3 GHz using a Keysight N9918A Fieldfox microwave analyzer. Scattering parameters can be effectively used for the Fat-IBC channel characterisation since the anatomical lengths are in the accessible range of any multiport network analyzer. This provides better accuracy in measurements unlike traditional antenna communication link measurements where two independent transmitter and receiver systems are used.

To evaluate the antennas/fat channel performance with modulated signals, we used Rohde & Schwarz (R&S) SMCV100B vector signal generator (VSG) and FSVA3000 vector signal and spectrum analyzer (VSA). Measurements of bit error rate (BER) vs. normalized SNR (E_b/N_0) were used to compare performance of different digital modulation schemes.

A 1 MSamples/s PRBS 9-encoded data stream with an RRC filter setting of 0.22 was used with all digital modulation formats (BPSK to 512-QAM, IEEE 802.11n uses up to 64-QAM). The output power of the VSG was set to 10 dBm at the 2.45 GHz target frequency. The E_b/N_0 using added additive white Gaussian noise (AWGN) was swept and the BER down to 10^{-6} was recorded for the different modulations.

E. IEEE 802.11n link

For the 802.11n link, we utilized two Raspberry Pi Compute Module 4 units (CM4102008) [28]. This particular Raspberry Pi model is equipped with a wireless module based on the Cypress Semiconductor CYW43455 [29], which — unlike the wireless module on the ordinary Raspberry Pi 4 — has a U.FL connector for an external antenna. A "DFRobot IoT Carrier Board Mini" expansion board provided power and a gigabit Ethernet connection, which was used to communicate with a host computer.

RF leakage from the U.FL connector and adapter cable was identified as a possible concern. To address this, the units were mounted in 3D-printed cases wrapped in a 30-µm thick aluminum sheet. Each case was then placed on an absorber sheet, with another absorber sheet on top. The U.FL-to-SMA connections were also wrapped with the aluminum sheet.

Raspberry Pi OS Lite version 10 (32-bit, Linux kernel version 5.10.103) was installed on the on-board storage. The host access point daemon (Hostapd) software was used on one Raspberry Pi to broadcast a service set identifier (SSID), with which the second Raspberry Pi joined the network. The Hostapd (version 2.9) source code was modified to allow 40 MHz bandwidths in the 2.4 GHz band regardless of any surrounding interference from overlapping stations (which technically violates IEEE 802.11-2012, 10.14.3.2). We specified the desired wireless channel and activated the HT20 and HT40 capabilities in the Hostapd configuration file. The data rate was measured with the "Iperf3" tool in User Datagram Protocol (UDP) mode as an average of a number of measurements performed within a time duration of 60 seconds (block size 1448 bytes).

The radio transmission power and guard interval length were set in firmware with the help of the "WL" command-line tool from Cypress Semiconductor [30], after which we recorded the auto-negotiated data rate and its associated HT MCS setting with Iperf3. Similarly, the achieved data rate at HT MCS 0–7 was recorded in the same way, with the "WL" tool "forcing" the radio to operate in a specific HT MCS mode.

III. Results

In this section, the performance of the Fat-IBC link for high-speed data transmission using different antenna combinations is evaluated using s-parameter measurements, modulated high-speed data measurements, and creating a WLAN link through the Fat-IBC material using two Raspberry Pis connected to the inbody and onbody antennas. All radio measurements used the same experimental setup (phantoms and shielded chamber) except for the length of the phantoms (10, 20, 30 cm) and the antennas (onbody and inbody) combinations.

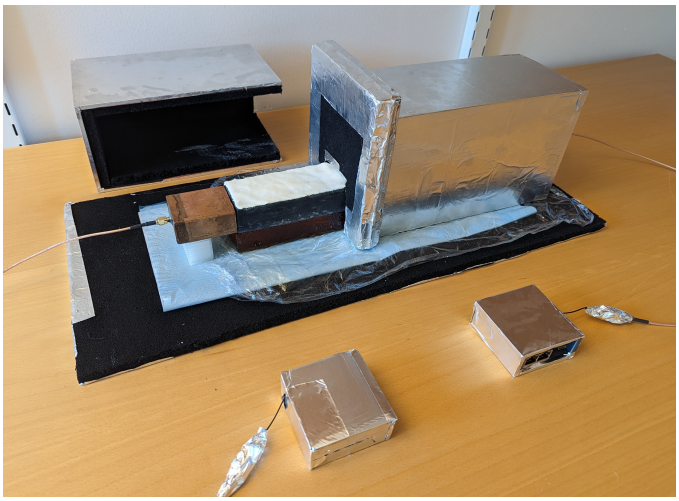

Fig. 4. The shielded chamber with one chamber segment at the side, exposing the three-layer phantom and one of the TOPAs inside. In front are the two Raspberry Pis inside aluminum-clad cases.

Fig. 4 shows the actual measurement setup with the shielded chamber (here opened for inspection), a phantom, and a TOPA.

A. Case 1: inbody-to-inbody antennas

Fig. 5, (a) and (b), show the measured input (s_{11}) and output (s_{22}) reflection coefficients for the implant-to-implant antenna configuration. These parameters are used to estimate the matching or the effectiveness of the energy coupling of the signal from the antenna to the fat layer. The values below –25 dB indicate excellent coupling for the 10 cm and 20 cm phantoms. For the 30 cm phantom, while still below –15 dB, the measured s_{11} and s_{22} indicate a slightly higher level of impedance mismatch. Fig. 5 (c) shows the transmission coefficient (s_{21}), which is interpreted as the signal loss in the fat channel. It scales almost linearly (in dB) as 1 dB/cm loss at the target frequency 2.45 GHz, consistent with our previous observations [15].

The radio link performance, measured as described in Section II-D, for different modulation schemes are shown in Fig. 6 for the 30 cm phantom (the shorter phantoms showed almost identical performance). We could reach BER $< 10^{-6}$ for all tested modulations.

To test the performance using an established wireless communication standard and tools, we measured the fat-channel link performance with an IEEE 802.11n network as described in Section II-E. By connecting the two Raspberry Pis to the different antenna combinations, a local auto-negotiating peer-to-peer network was created. For the 30 cm phantom with the implanted antennas inside the shielded chamber, we obtained a 91.6 Mb/s link (MCS 7, HT40).

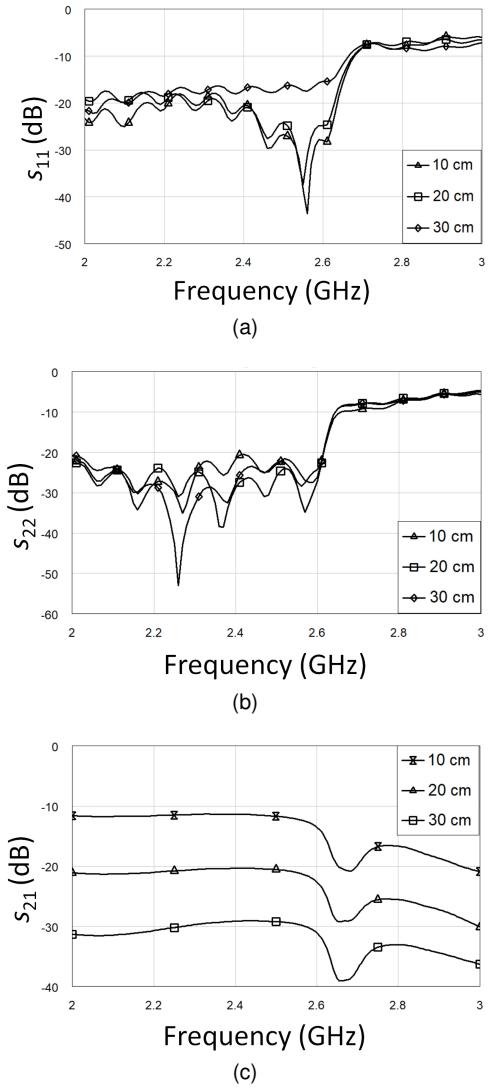

Fig. 5. Case 1: (a) input reflection coefficient (s_{11}), (b) output reflection coefficient (s_{22}), (c) transmission coefficient (s_{21}) for the three different phantom lengths.

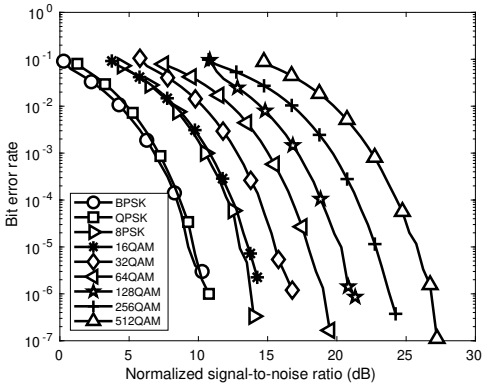

Fig. 6. Case 1: BER vs. E_b/N_0 for different modulation schemes.

We also swept MCS, forcing the modulation settings for 20 and 40 MHz bandwidths. The resulting data rates are shown in Fig. 7. For 20 MHz bandwidth, we obtained up to 58.0 Mb/s, while increasing the bandwidth to 40 MHz saw the data rate saturate at 92 Mb/s for MCS 5–7 (64-QAM).

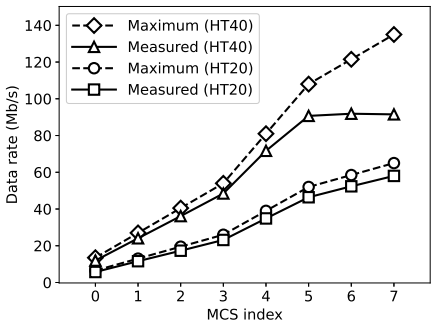

Fig. 7. Case 1: Date rate vs. MCS index for bandwidths of 20 MHz and 40 MHz, 30 cm phantom length.

B. Case 2: inbody-to-onbody antennas

Fig. 8 shows the measured s_{11} and s_{22} parameters for the inbody-to-onbody antenna configuration. The input (s_{11}) and output (s_{22}) reflection coefficients are now asymmetrical, with high reflection coefficients for port 2, which is the onbody antenna. s_{11} shows a good coupling using the implanted antenna (less than –15 dB), while the s_{22}, the onbody antenna shows reduced coupling (–4 dB) to the fat layer. The s_{21}, Fig. 8(c) shows losses at 2.45 GHz proportional to the phantom lengths, similar to the inbody-to-inbody antennas but with higher fixed losses because of the less good coupling (s_{22}) from the onbody antenna to the phantom.

The radio link performance, Fig. 9, is almost identical to the implant-to-implant case, although at 512-QAM, the performance deteriorates at low BER.

When connecting the two Raspberry Pis to the in-body/onbody antennas, an almost identical link speed of 91.8 Mb/s (MCS 7, HT40) as the inbody-to-inbody case (91.6 Mb/s) was obtained.

Sweeping the MCS for 20 and 40 MHz bandwidth, as shown in Fig. 10, shows similar performance to the previous case, with almost 60 Mb/s performance for 20 MHz bandwidth, and around 92 Mb/s using MCS 5–7 (64-QAM) at 40 MHz bandwidth.

C. Case 3: onbody-to-onbody antennas

The s-parameters for the case with dual onbody antennas show not so good coupling to the skin/fat/muscle phantom, as evident from Fig. 11, which also cancels out possible variations of matching to the different phantoms of different lengths. The s_{21}, Fig. 11(b), again scales reasonably well with the phantom length.

The radio link performance, Fig. 12(c), shows clear degradation of BER with the 30 cm phantom for 32-QAM and higher-order modulations. In comparison, the 20 cm phantom, Fig. 12(b), shows some degradation for 128-QAM and higher modulation, while the 10 cm phantom, Fig. 12(a), shows good performance for all modulations. Considering the losses in the link through the different phantoms and the settings of the signal analyzer during the measurements, this degradation is likely due to too weak input signal for the analyzer to correctly demodulate the received signals.

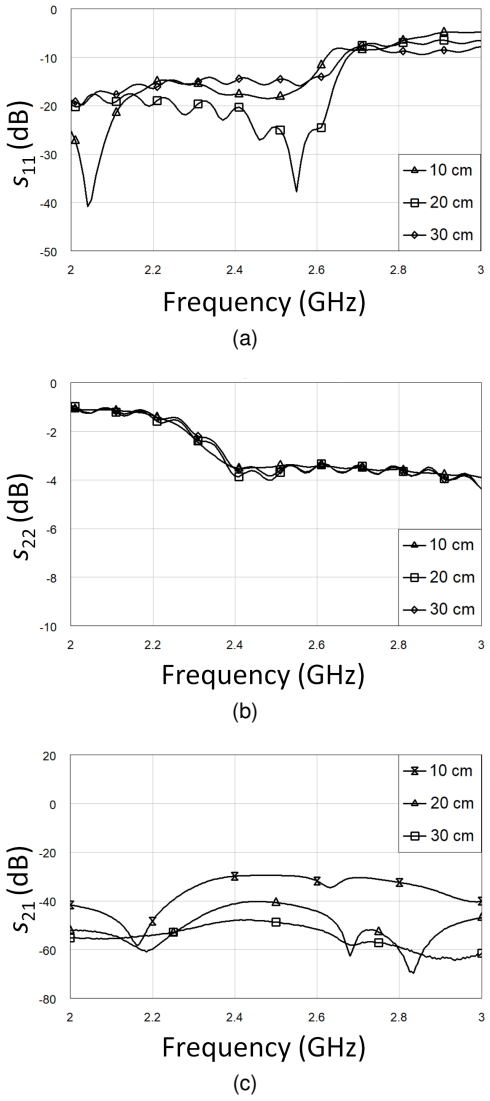

Fig. 8. Case 2: inbody-to-onbody antennas: (a) input reflection coefficient (s_{11}), (b) output reflection coefficient (s_{22}), (c) transmission coefficient (s_{21}) for the three different phantom lengths.

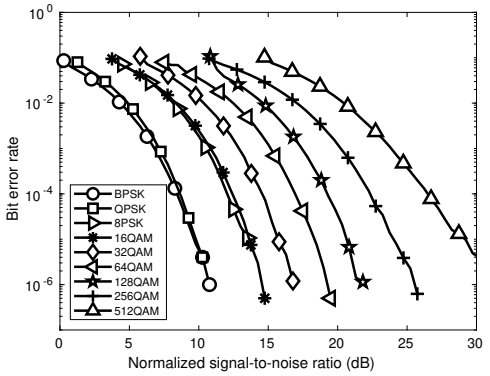

Fig. 9. Case 2: BER vs. E_b/N_0 for different modulation schemes.

For the Raspberry Pi link speed, also for this case it was possible to achieve a link speed of 91.6 Mb/s (MCS 7, HT40).

Sweeping the MCS for 20 and 40 MHz bandwidth, as shown in Fig. 13, shows similar performance as the previous cases, with 58 Mb/s performance for 20 MHz bandwidth, and 92 Mb/s using MCS 5–7 (64-QAM) at 40 MHz bandwidth.

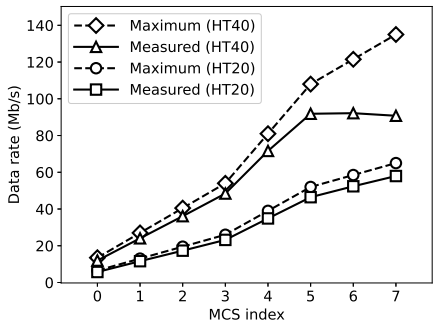

Fig. 10. Case 2: Date rate vs. MCS index for bandwidths of 20 MHz and 40 MHz, 30 cm phantom length.

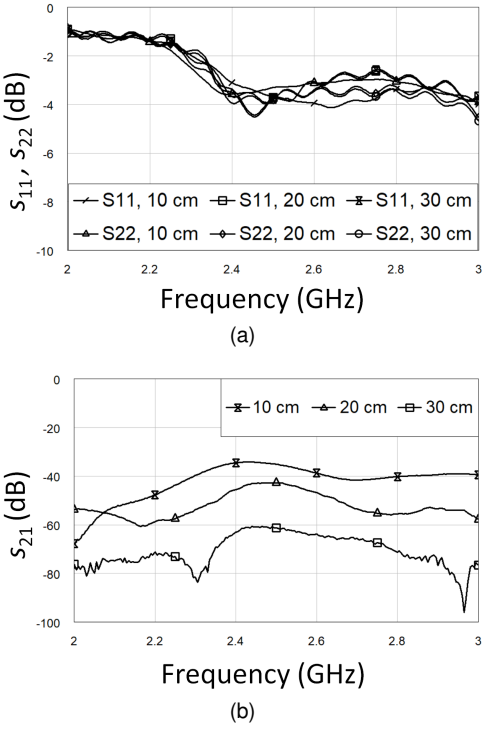

Fig. 11. Case 3: onbody-to-onbody antennas: (a) input reflection coefficient (s_{11}) and output reflection coefficient (s_{22}), (b) transmission coefficient (s_{21}) for the three different phantom lengths.

IV. Discussion

The small-signal characterization of the phantoms with the different antenna combinations shows a loss for microwave signal of around 1 dB/cm in the fat channel. The inbody antennas give excellent coupling to the fat channel, while the onbody (on the skin) antennas need to be improved to better couple the signal to/from the fat channel without high insertion losses.

The BER measurements show that, except when using dual on-body antennas with the longer phantoms, the Fat-IBC link is very linear and can handle modulations as complex as 512-QAM without any significant degradation of the BER.

For the high-speed data communication, the throughput saturates at 92 Mb/s for all different phantoms and antenna

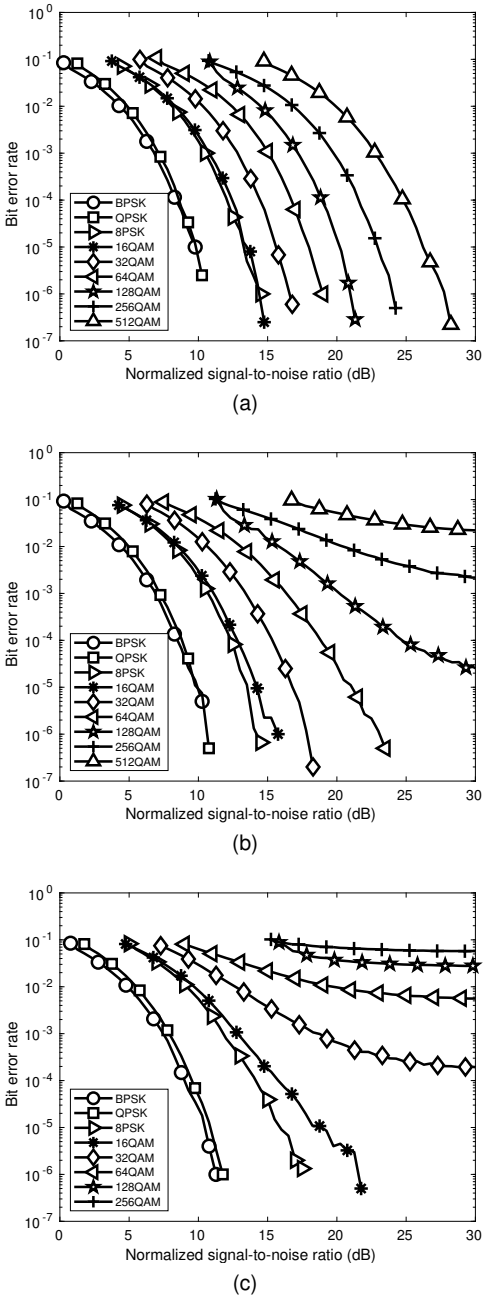

Fig. 12. Case 3: BER vs. E_b/N_0 for different modulation schemes: (a) 10 cm phantom length, (b) 20 cm phantom length, (c) 30 cm phantom length.

combinations (Fig. 7, 10, and 13). This is not the upper limit according to the IEEE 802.11n standard, see Table I, but the SDIO interface on the CYW43455 wireless module likely limits the throughput [29]. The results show that a Fat-IBC link, using low-cost off-the-shelf hardware and established IEEE 802.11 wireless communication, can achieve high-speed data communication within the body, and the data rate is among the fastest measured with intrabody communication. Table II shows a comparison with other similar inbody communication.

For the case with onbody antennas using the longest phantom of 30 cm, from the BER measurements plot, Fig. 12(a), one would think that there would be a degradation in the full link speed, but a WLAN link speed of 92 Mb/s data using

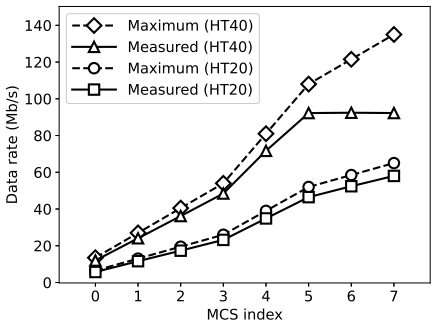

Fig. 13. Case 3: Date rate vs. MCS index for bandwidths of 20 MHz and 40 MHz, 30 cm phantom length.

64-QAM modulation at 40 MHz bandwidth was still achieved for this case. In fact, the BER measurements (see Section II-D) were performed with a generic 1 MSamples/s data stream without any advanced coding or error correction that otherwise would be present in an actual IEEE 802.11n system [33], so the BER results may not in this case be a clear indication on the achievable data rate when used with a full IEEE 802.11n system.

For the used phantoms and antennas, we did not observe a limitation in the obtained link speed for IEEE 802.11n that could be correlated to the antennas or length of the phantoms. By using only the inbody antennas (Case 1), 30 dB is gained in the link budget compared to the onbody antennas (Case 3), which would extend the possible link distance by 30 cm. As the losses are proportional to the phantom length, by increasing the transmitted power, the fat channel length may also be extended proportionally without degrading the throughput, while considering applicable specific absorption rate (SAR) limitations.

V. Summary, Future Work

In this paper, we have explored Fat-IBC as a wireless communication link for high-speed intrabody communication (IBC) using inbody (implanted) topology-optimized planar antennas (TOPAs) and ring-shaped onbody (on the skin) antennas.

The signal properties of the antennas and the link at microwave frequencies were characterized by s-parameter measurements. BER measurements were used to show that, except when using dual on-body antennas with the longer phantoms, the Fat-IBC link is very linear and can handle modulations as complex as 512-QAM without any sigificant degradation of the BER.

To reach 64 Mb/s data communication speed, IEEE 802.11n wireless communication in the 2.4 GHz band was used to establish a link inside the body, emulated by phantoms of different lengths, and measured in a shielded chamber to suppress unwanted propagation paths and interference from external sources.

For all antenna combinations and phantoms lengths, link speeds of 92 Mb/s were achieved using the 40 MHz bandwidth provided by the IEEE 802.11n standard, which is among the

TABLE II
COMPARISON WITH OTHER SIMILAR INBODY COMMUNICATION

Reference	[31]	[32]	[10]	This work
Year	2014	2019	2020	2023
Method	CC-BCC	GC-BCC	CC-BCC	Fat-IBC
Speed	60 Mb/s @ 100 cm	100 Mb/s @ 10 cm (est)	150 Mb/s @ 20 cm 10 Mb/s @100 cm	92 Mb/s @ 30 cm
Hardware	65 nm CMOS	180 nm CMOS	65 nm CMOS	"off-the-shelf"
Modulation	3-level Walsh	Bipolar RZ	DFE	802.11n
Medium	Human body	Porcine	Human body	Phantom
Frequency band (MHz)	Baseband	Baseband	Baseband	2400–2450
Bandwidth (MHz)	up to 80	100	150	40

highest speed measured with intrabody communication, and most likely limited by the used radio circuits. This shows that Fat-IBC, using low-cost off-the-shelf hardware and established IEEE 802.11 wireless communication, can achieve high-speed data communication with intrabody communication for wearable and implantable sensor networks.

Future work includes similar experiments at 5.8 GHz (i.e. IEEE 802.11ac) and larger bandwidths, increased transmit power, optimized onbody antennas, and other phantoms with different geometries to explore the limits of Fat-IBC communication.

ACKNOWLEDGMENT

The authors would like to thank Rohde & Schwarz Sverige AB for access to the vector signal instruments, and Bappaditya Mandal and Arvind Selvan Chezhian for their significant involvement in the experimental setup. The authors are also thankful to Roger L. Karlsson for his valuable comments on the manuscript.

REFERENCES

[1] M. Chen, S. Gonzalez, A. Vasilakos, H. Cao, and V. C. M. Leung, "Body area networks: A survey," *Mobile Networks and Applications*, vol. 16, no. 2, pp. 171–193, Apr, 2011.

[2] X. Lai, Q. Liu, X. Wei, W. Wang, G. Zhou, and G. Han, "A survey of body sensor networks," *Sensors*, vol. 13, no. 5, pp. 5406–5447, 2013.

[3] S. Marathe, D. Zeeshan, T. Thomas, and S. Vidhya, "A wireless patient monitoring system using integrated ECG module, pulse oximeter, blood pressure and temperature sensor," in *2019 International Conference on Vision Towards Emerging Trends in Communication and Networking (ViTECoN)*, 2019, pp. 1–4.

[4] S.-H. Kim and K. Chung, "Emergency situation monitoring service using context motion tracking of chronic disease patients," *Cluster Computing*, vol. 18, no. 2, pp. 747–759, 2015.

[5] S. Movassaghi, M. Abolhasan, J. Lipman, D. Smith, and A. Jamalipour, "Wireless body area networks: A survey," *IEEE Communications Surveys & Tutorials*, vol. 16, no. 3, pp. 1658–1686, 2014.

[6] IEEE LAN/MAN Standards Committee. (2023, Jan 15.) IEEE 802.15 working group for wireless specialty networks (WSN). [Online]. Available: https://www.ieee802.org/15/

[7] Y. Song, Q. Hao, and K. Zhang, "Review of the Modeling, Simulation and Implement of Intra-body Communication," *Defence Technology*, vol. 9, no. 1, pp. 10–17, 2013.

[8] W. J. Tomlinson, S. Banou, C. Yu, M. Stojanovic, and K. R. Chowdhury, "Comprehensive survey of galvanic coupling and alternative intrabody communication technologies," *IEEE Communications Surveys & Tutorials*, vol. 21, no. 2, pp. 1145–1164, 2019.

[9] B. Jaafar, J. Neasham, and P. Degenaar, "What ultrasound can and cannot do in implantable medical device communications," *IEEE Reviews in Biomedical Engineering*, vol. 16, pp. 357–370, 2023.

[10] J.-H. Lee, J. Ko, K. Kim, M. Choi, J.-Y. Sim, H.-J. Park, and B. Kim, "A body channel communication technique utilizing decision feedback equalization," *IEEE Access*, vol. 8, pp. 198 468–198 481, 2020.

[11] "An interface connects," *Nature Electronics*, vol. 6, no. 2, pp. 89–89, Feb. 2023. [Online]. Available: https://doi.org/10.1038/s41928-023-00938-8

[12] Horizon 2020. (2023, Jan 15.) Modern BCI — B-CRATOS. [Online]. Available: https://www.b-cratos.eu/

[13] N. B. Asan, D. Noreland, E. Hassan, S. Redzwan Mohd Shah, A. Rydberg, T. J. Blokhuis, P.-O. Carlsson, T. Voigt, and R. Augustine, "Intrabody microwave communication through adipose tissue," *Healthcare Technology Letters*, vol. 4, no. 4, pp. 115–121, 2017.

[14] D. Andreuccetti, R. Fossi, and C. Petrucci. (2023, Jan 15.) IFAC-CNR, Florence, Italy. [Online]. Available: http://niremf.ifac.cnr.it/tissprop/

[15] N. B. Asan, J. Velander, Y. Redzwan, R. Augustine, E. Hassan, D. Noreland, T. Voigt, and T. J. Blokhuis, "Reliability of the fat tissue channel for intra-body microwave communication," in *2017 IEEE Conference on Antenna Measurements and Applications (CAMA)*, 2017, pp. 310–313.

[16] N. B. Asan, E. Hassan, M. D. Perez, L. Joseph, M. Berggren, T. Voigt, and R. Augustine, "Fat-intrabody communication at 5.8 GHz: Verification of dynamic body movement effects using computer simulation and experiments," *IEEE Access*, vol. 9, pp. 48 429–48 445, 2021.

[17] IEEE Working Group for WLAN Standards. (2023, Jan 15.) IEEE 802.11 wireless local area networks. [Online]. Available: https://www.ieee802.org/11/

[18] Wikipedia. (2023, Feb 26.) IEEE 802.11n-2009. [Online]. Available: https://en.wikipedia.org/wiki/IEEE_802.11n-2009

[19] *IEEE Standard for Information technology — Local and metropolitan area networks — Specific requirements — Part 11: Wireless LAN Medium Access Control (MAC) and Physical Layer (PHY) Specifications Amendment 5: Enhancements for Higher Throughput*, IEEE Std. 802.11n-2009, 2009.

[20] N. B. Asan, C. P. Penichet, S. Redzwan Mohd Shah, D. Noreland, E. Hassan, A. Rydberg, T. J. Blokhuis, T. Voigt, and R. Augustine, "Data packet transmission through fat tissue for wireless intrabody networks," *IEEE Journal of Electromagnetics, RF and Microwaves in Medicine and Biology*, vol. 1, no. 2, pp. 43–51, 2017.

[21] N. B. Asan, E. Hassan, J. Velander, S. R. Mohd Shah, D. Noreland, T. J. Blokhuis, E. Wadbro, M. Berggren, T. Voigt, and R. Augustine, "Characterization of the fat channel for intra-body communication at R-band frequencies," *Sensors*, vol. 18, no. 9, p. 2752, 2018.

[22] E. Hassan, D. Noreland, E. Wadbro, and M. Berggren, "Topology optimisation of wideband coaxial-to-waveguide transitions," *Scientific reports*, vol. 7, no. 1, pp. 1–9, 2017.

[23] B. K. Kanaujia and A. K. Singh, "Analysis and design of gap-coupled annular ring microstrip antenna," *International Journal of Antennas and Propagation*, vol. 2008, 2008.

[24] L. Joseph, M. D. Perez, and R. Augustine, "Development of Ultra-Wideband 500 MHz–20 GHz Human Skin Phantoms for Various Microwaves Based Biomedical Applications," in *2018 IEEE Conference on Antenna Measurements & Applications (CAMA)*, 2018, pp. 1–3.

[25] L. Joseph, "Development of ultra-wide band 500 MHz–20 GHz heterogeneous multi-layered phantom comprises of human skin, fat and muscle tissues for various microwaves based biomedical application," M.S. thesis, Dept. Elect. Eng, Uppsala Univ., Uppsala, Sweden, 2019. [Online]. Available: https://urn.kb.se/resolve?urn=urn:nbn:se:uu:diva-402458

[26] Keysight Technologies. 8507E dielectric probe kit. Accessed: Jan. 15, 2023. [Online]. Available: https://www.keysight.com/us/en/product/85070E/dielectric-probe-kit.html

[27] P. K. B. Rangaiah, R. L. Karlsson, A. S. Chezhian, L. Joseph, B. Mandal, B. Augustine, M. Mani, M. D. Perez, T. Voigt, and R. Augustine, "Realization of a portable semi-shielded chamber for evaluation of fat-intrabody communication," *IEEE Access*, pp. 1–1, 2023.

[28] "Raspberry Pi Compute Module 4 — a Raspberry Pi for deeply embedded applications," Raspberry Pi Ltd., rev. 2022-06-07.

[29] "CYW43455 — single-chip 5G WiFi IEEE 802.11n/ac MAC/baseband/radio with integrated Bluetooth 5.0," Cypress Semiconductor, Document No.: 002-15051 Rev. *O.

[30] "WL tool for embedded 802.11 systems — CYW43xx technical information," Cypress Semiconductor, Document No.: 002-23156 Rev. **.

[31] C. K. Ho, J. H. Cheong, J. Lee, V. Kulkarni, P. Li, X. Liu, and M. Je, "High bandwidth efficiency and low power consumption Walsh code implementation methods for body channel communication," *IEEE Transactions on Microwave Theory and Techniques*, vol. 62, no. 9, pp. 1867–1878, 2014.

[32] Y. Jeon, C. Jung, S.-I. Cheon, H. Cho, J.-H. Suh, H. Jeon, S.-T. Koh, and M. Je, "A 100 Mb/s galvanically-coupled body-channel-communication transceiver with 4.75 pJ/b TX and 26.8 pJ/b RX for bionic arms," in *2019 Symposium on VLSI Circuits*, 2019, pp. C292–C293.

[33] N. Ravindranath, I. Singh, A. Prasad, and V. Rao, "Performance evaluation of IEEE 802.11ac and 802.11n using NS3," *Indian Journal of Science and Technology*, vol. 9, no. 26, pp. 1–8, 2016.